The dynamic properties of a nuclear coactivator binding domain are evolutionarily conserved

Elin Karlsson[1], Frieda A. Sorgenfrei[1,†], Eva Andersson[1], Jakob Dogan[1], Per Jemth[1,*], and Celestine N. Chi[1,2,*]

[1]Department of Medical Biochemistry and Microbiology, Uppsala University, BMC Box 582, SE-75123 Uppsala, Sweden.

[2]Department of Pharmaceutical Biosciences, Uppsala University, BMC Box 582, SE-75123 Uppsala, Sweden

[†]Present address: acib GmbH, Krenngasse 37, 8010 Graz c/o University of Graz, Institute of Chemistry, NAWI Graz, BioTechMed Graz, Heinrichstrasse 28, 8010 Graz, Austria

*Correspondence to

Celestine Chi, Celestine.Chi@imbim.uu.se

Per Jemth, Per.Jemth@imbim.uu.se

ABSTRACT

Evolution of proteins is constrained by their structure and function. While there is a consensus that the plasticity of intrinsically disordered proteins relaxes the structural constraints on evolution there is a paucity of data on the molecular details of these processes. The Nuclear co-activator binding domain (NCBD) from CREB-binding protein is a protein-protein interaction domain, which contains a hydrophobic core but is verging on being intrinsically disordered. These highly dynamic 'borderline' properties of NCBD makes it an interesting model system for evolutionary structure-function investigation of intrinsically disordered proteins. We have here compared the structure and biophysical properties of an ancient version of NCBD present in a bilaterian animal ancestor living around 600 million years ago with extant human NCBD. Using a combination of NMR spectroscopy, circular dichroism and kinetic methods we show that NCBD has retained its structure and dynamic biophysical properties in the ligand-free state in the evolutionary lineage leading from the last common bilaterian ancestor to humans. Our findings suggest that the dynamic properties of NCBD are subject to positive selection and thus important for its function, which includes mediating several distinct protein-protein interactions.

Introduction

Evolution has shaped proteins into a wide spectrum of structure, stability and dynamics, with fully disordered proteins at one end of the scale and well-folded globular proteins at the other one (*1*). It is becoming clear that dynamic properties *per se* are important for protein function (*1–3*) but it is not trivial to prove that the dynamics are essential for biological function and not merely a general property of proteins. The Nuclear Coactivator Binding Domain (NCBD) is a small (approximately 50 residues) domain from CREB-binding protein (CBP, also called CREBBP), which is a transcriptional coactivator with histone acetylase activity and present in all animals (*4*). The NCBD domain has a hydrophobic core, but is very dynamic and even verging on being intrinsically disordered (*5–7*). It has therefore been described as "molten-globule-like" (*8–11*). The fact that NCBD possesses properties of both intrinsically disordered and globular proteins makes it an interesting system for assessing the role of dynamics in protein structure and how it modulates function. We have previously subjected NCBD to "evolutionary biochemistry" (*12*, *13*). Thus, we resurrected and characterized ancestral versions of NCBD and its protein ligand CBP-Interacting Domain (CID) from the NCOA1, 2 and 3 protein family (with three members in human called Src1, Tif2 and ACTR, respectively) to address the evolution of affinity in this protein-protein interaction. The oldest "maximum likelihood" (ML) NCBD variant we could resurrect was present before the Cambrian period, some 540-600 million years ago, in the common ancestor of all present-day animals with bilaterian symmetry. These animals are divided into deuterostomes and protostomes (D/P) and the ancestral NCBD domain is denoted $NCBD_{D/P}^{ML}$. It was shown to bind the CID domain with relatively low affinity ($K_d \sim$ 1-5 μM) whereas more recent variants of NCBD in the vertebrate lineage

63 (ca. 440 million years ago) had acquired present-day affinity for CID (K_d ~ 0.1-0.2 μM).
64 Structural characterization of ancestral and present-day CID/NCBD complexes showed
65 that the increase in affinity observed for more modern NCBD variants was due to a
66 combination of factors. These include several new interactions driving structural and
67 dynamic changes in the complex, such as formation of a third α helix in CID upon
68 interaction (*13*). In the present paper, we investigate the structural and biophysical
69 properties of the ligand-free state of the ancestral Cambrian-like low-affinity
70 $NCBD_{D/P}^{ML}$ and compare it to that of high-affinity present-day $NCBD_{Human}$ to track the
71 evolution of structure and dynamics and their relation to function. The comparison
72 reveals that the overall properties of the ancestral $NCBD_{D/P}^{ML}$ domain are very similar
73 to those of the present-day $NCBD_{Human}$. In general, conservation implies function. Thus,
74 this conservation of a highly dynamic structure and molten-globule like properties
75 suggest that these features are under positive selection and hence that dynamics are
76 indeed important for the biological function of NCBD.
77
78
79 **Results**
80
81 **The structures of ancient $NCBD_{D/P}$ and extant $NCBD_{Human}$ are similar but not**
82 **identical.** Because of its dynamic properties it is challenging to solve the structure of
83 ligand-free NCBD (*8*). First, we performed experiments with ^{15}N labeled $NCBD_{D/P}^{ML}$.
84 We discovered by serendipity that low pH significantly improved the quality of the
85 $^{1}H^{15}N$ heteronuclear single quantum coherence (HSQC) spectrum resulting in well
86 dispersed peaks for $NCBD_{D/P}^{ML}$ (Fig. 1), and allowing for a near complete assignment
87 of the backbone and side-chain residues from NMR 3D experiments using ^{13}C and ^{15}N

88 labeled samples. The NMR structure was thus determined at pH 2.4 by measuring 3D
89 1H-1H $^{13}C/^{15}N$ resolved NOESY experiments for distance restraints determination and
90 $^{3}J_{HNHA}$ for dihedral angle determination. The structure of $NCBD_{D/P}^{ML}$ was found to be
91 overall consistent with that of the free (*8*) and bound $NCBD_{Human}$ (*6*) and bound
92 $NCBD_{D/P}^{ML}$ determined at pH 6.8 (*13*) (Fig. 1). However, a detailed comparison
93 between $NCBD_{D/P}^{ML}$ and $NCBD_{Human}$ shows that the orientation of helix 1 (α1) and
94 helix 3 (α3) differ between the structures. Upon structural alignment of $NCBD_{Human}$
95 and $NCBD_{D/P}^{ML}$, we observed that both the α1 and α3 from $NCBD_{D/P}^{ML}$ are slightly
96 tilted away relative to that of $NCBD_{Human}$. We also observed that for CID-bound
97 $NCBD_{D/P}^{ML}$ and free $NCBD_{D/P}^{ML}$ the α3 displayed structural rearrangements (Fig. 2).
98
99 The amino acid sequence of $NCBD_{D/P}^{ML}$ was reconstructed using phylogenetic
100 methods[4]. The probability is low that the resulting maximum likelihood sequence is
101 identical to the actual sequence present in the ancestor. Thus, $NCBD_{D/P}^{ML}$ is rather one
102 of a large number of likely ancestral variants with similar properties. We wondered if
103 errors in the sequence of $NCBD_{D/P}^{ML}$ resulted in the differences we observe in helix α1
104 and α3 compared to $NCBD_{Human}$. To investigate this further, and to test how structurally
105 robust the dynamic NCBD domain is, we performed a control experiment where we
106 expressed, purified and characterized an alternative $NCBD_{D/P}$ variant denoted
107 $NCBD_{D/P}^{AltAll}$. In this $NCBD_{D/P}^{AltAll}$ variant, all residues with a posterior probability
108 lower than around 0.9 (*12*) were replaced with the second most likely residue at that
109 position. For example, residue 2107 is His with 87% probability and Gln with 12%
110 probability in the ancestral $NCBD_{D/P}$. Thus, $NCBD_{D/P}^{ML}$ has a His in position 2107 and
111 $NCBD_{D/P}^{AltAll}$ a Gln residue. $NCBD_{D/P}^{AltAll}$ can be considered a "worst case scenario"
112 variant and a good control of the robustness of conclusions drawn from resurrection

113 experiments. If ML and AltAll variants display similar properties it is very likely that
114 the actual ancestral protein shares these properties as well. Because of this, an AltAll
115 variant is a convenient alternative to combinations of point mutations (*14*).
116 $NCBD_{D/P}^{AltAll}$ contains six substitutions as compared to $NCBD_{D/P}^{ML}$ (Fig. 1). Three of
117 the differences between $NCBD_{D/P}^{ML}$ and $NCBD_{D/P}^{AltAll}$ are in the N-terminus, but only
118 one of these is in a structured region, a Gln2065→Pro at the beginning of α1. The other
119 three differences are Ser2078→Asn in the loop between α1 and α2, a solvent exposed
120 Gln2088→His in α2 and His2108→Gln at the C-terminus. We solved the NMR
121 structure of $NCBD_{D/P}^{AltAll}$ (Fig. S1) and found that it folds into a similar structure as the
122 other NCBD domains. The overall RMSD between $NCBD_{D/P}^{AltAll}$ and $NCBD_{D/P}^{ML}$ was
123 7.9 Å. As a comparison, the overall RMSD between $NCBD_{Human}$ and $NCBD_{D/P}^{AltAll}$ or
124 $NCBD_{D/P}^{ML}$ were 4.5 Å and 7.0 Å, respectively. Detailed inspection of the structures
125 revealed differences in the backbone between $NCBD_{D/P}^{ML}$ and $NCBD_{D/P}^{AltAll}$,
126 especially in the orientations of the helices. An overlay of the structures of
127 $NCBD_{D/P}^{AltAll}$, $NCBD_{D/P}^{ML}$, and $NCBD_{Human,}$ shows differences between α1, α2 and α3
128 (Fig. S1). One reason for the differences is that there are several long-range NOEs in
129 $NCBD_{D/P}^{AltAll}$ that are not present in $NCBD_{D/P}^{ML}$, between the following pairs of
130 residues: 2068/2082, 2069/2080, 2070/2083 and 2071/2099. There is also an NOE
131 between Ile2062 Hγ, and Pro2065 Hα, two of the substituted residues in $NCBD_{D/P}^{AltAll}$.
132 However, there appears to be a consistency in the hydrophobic core of both $NCBD_{D/P}^{ML}$
133 and $NCBD_{D/P}^{AltAll}$ since the single Phe residue at position 2100 is packed and buried in
134 a similar fashion in the two variants. Phe2100 is stabilized by Leu2090 in $NCBD_{D/P}^{ML}$,
135 and both Ile2089 and Leu2090 in $NCBD_{D/P}^{AltAll}$ (Fig. 3). Interestingly, this is the same
136 kind of packing that was observed in the free $NCBD_{human}$ domain (*8*), suggesting
137 conserved features in the hydrophobic core.

138

139 Despite the differences discussed in the previous paragraph, the overall biophysical
140 properties of $NCBD_{D/P}^{ML}$ and $NCBD_{D/P}^{AltAll}$ were found to be similar (Fig. S2)
141 corroborating the overall similarity seen with the NMR structures. Specifically, to test
142 the affinity of $NCBD_{D/P}^{AltAll}$ for CID, we expressed and purified ML and AltAll
143 versions of its ligand CID_{1R} based on our previous reconstruction (*8*). K_d values of all
144 four combinations ($NCBD_{D/P}^{ML}$ and $NCBD_{D/P}^{AltAll}$ with CID_{1R}^{ML} and CID_{1R}^{AltAll}) were
145 between 2-9 μM (Fig. S2a), which is in the same range as previous estimates of affinity
146 of the ancestral complex (*12*, *13*). Furthermore, the stability as monitored by urea
147 denaturation (Fig. S2b) and thermal denaturation (Fig. S2c-d) were similar for
148 $NCBD_{D/P}^{ML}$ and $NCBD_{D/P}^{AltAll}$. Thus, based on the highly similar biophysical
149 properties of $NCBD_{D/P}^{ML}$ and $NCBD_{D/P}^{AltAll}$ we conclude that our conclusions are
150 robust with regard to the uncertainty in the reconstructed sequence.

151

152 **Ancient $NCBD_{D/P}$ and extant $NCBD_{Human}$ display similar pH dependence with**
153 **regard to structure and stability.** Since the $NCBD_{D/P}^{ML}$ structure was determined at
154 low pH, we next investigated how pH influences the fold and stability. First, we
155 performed ^{1}H-^{15}N HSQC-monitored pH titrations of $NCBD_{D/P}^{ML}$ and compared them
156 to those of $NCBD_{Human}$ at different pH values (Fig. 4). The NMR titration experiments
157 showed that $NCBD_{D/P}^{ML}$ is as folded at low pH as it is at high pH values. However, the
158 peaks (^{1}H-^{15}N) are much sharper (reduced line-width) at lower pH values indicating
159 less conformational heterogeneity. Second, the CD-monitored urea denaturation
160 experiments showed identical stability pattern at two pH values (3.0 and 7.4) for both
161 ancient $NCBD_{D/P}^{ML}$ and extant $NCBD_{Human}$ (Fig. 4c and d, Supplementary table S1).
162 This indicates that while at lower pH the $NCBD_{D/P}^{ML}$ still exhibits the same stability as

163 at high pH values, there is a shift in conformational heterogeneity towards a single state
164 at low pH. Furthermore, whereas the apparent thermodynamic stability differs by
165 approximately 1 kcal mol^{-1} for ancient $NCBD_{D/P}^{ML}$ and extant $NCBD_{Human}$, both are
166 largely unaffected by a drop in pH to 3.0 (Supplementary Table S1). The observed
167 difference in stability between $NCBD_{D/P}^{ML}$ and $NCBD_{Human}$ appears to be a robust
168 result. Previous experiments suggested that the ancestral $NCBD_{D/P}^{ML}$ was slightly less
169 stable than younger and extant NCBD variants as judged by urea denaturation
170 experiments at pH 7.5 (*12*). However, the broad unfolding transition of NCBD resulting
171 from its small hydrophobic core leads to a large error in the $m_{D\text{-}N}$ value, which makes
172 it difficult to unequivocally determine the thermodynamic stability of the domain.
173 However, all present results (including experiments on the stabilized $NCBD_{D/P}^{ML}$
174 variant $NCBD_{D/P}^{T2073W}$ (Supplementary Table S1) agree well with the previous
175 experiments and we can therefore conclude with greater confidence that the ancestral
176 $NCBD_{D/P}^{ML}$ was less thermodynamically stable than evolutionarily younger variants.
177 Interestingly, with some exceptions (*15*, *16*), ancestral reconstructions often yield
178 proteins with higher thermostability, which correlates with thermodynamic stability,
179 than extant proteins, either due to a bias for stability in the reconstruction or due to
180 higher temperatures in past times (*17–21*), like during Cambrian (*22*, *23*). In any case,
181 ancestral NCBD appears to have populated the native state to a lesser extent than
182 present day human NCBD.
183
184 **Ancient $NCBD_{D/P}^{ML}$ and extant $NCBD_{Human}$ display similar temperature-**
185 **dependent structural changes.** Previous experiments demonstrated that $NCBD_{Human}$
186 shows an apparent non-cooperative unfolding behavior when subjected to increasing
187 temperatures, as monitored by CD (*6*, *8*). This behavior may result from a low $\Delta H_{D\text{-}N}$

188 value rather than a true non-cooperative unfolding. (The urea denaturation experiments
189 are consistent with a cooperative two-state unfolding.) We compared ^{1}H-^{15}N HSQC
190 and CD spectra, respectively, of $NCBD_{D/P}^{ML}$ and $NCBD_{Human}$ at different temperatures
191 (Fig. 5). In agreement with the previous data we observed that both variants unfold non-
192 cooperatively with temperature as monitored by the increase in molar ellipticity at 222
193 nm suggesting loss of α-helix as the temperature is increased. However, for both
194 $NCBD_{D/P}^{ML}$ and $NCBD_{Human}$ the signal is not completely lost even at 363 K (90°C)
195 underscoring that this is not a typical native to highly-disordered-denatured state
196 transition. Furthermore, ^{1}H-^{15}N HSQC spectra of $NCBD_{D/P}^{ML}$ at temperatures up to 333
197 K (60°C) show well dispersed peaks indicating a presumably globular, collapsed
198 architecture (Fig. S3) and corroborating the notion that NCBD retains structure at high
199 temperatures.
200
201 **Rate constants for (un)folding of ancient $NCBD_{D/P}^{ML}$ and extant $NCBD_{Human}$.** The
202 folding of human NCBD is complex, and, based on kinetic experiments on a human
203 NCBD variant, we proposed a three-state system involving 'native' NCBD (*i.e.*, the
204 solved structure), an intermediate state with unknown structure and a denatured state,
205 which likely retains significant structure under native conditions (*24*). Rate constants
206 in the same order was determined by relaxation dispersion NMR experiments by
207 Kjaergaard et al. (*10*) It is clear from the NMR experiments that low pH promotes the
208 native state of NCBD and that pH does not affect the thermodynamic stability as
209 monitored by urea denaturation experiments to any significant extent, neither for
210 $NCBD_{D/P}^{ML}$ nor $NCBD_{Human}$. Previous folding experiments on $NCBD_{Human}$ (*24*)
211 involving jumps from low to neutral pH thus resulted in small shifts in the equilibria
212 between the native, intermediate and denatured states yielding the observed kinetic

213 transients. In fact, a likely explanation for the better NMR spectra at low pH is that
214 there is less of the intermediate state under these conditions.
215
216 To further compare the biophysical properties of ancient $NCBD_{D/P}^{ML}$ and extant
217 $NCBD_{Human}$ we performed kinetic folding experiments using stopped-flow as well as
218 temperature-jump fluorescence spectroscopy. To achieve this we introduced a Trp at
219 position 2073 in $NCBD_{D/P}^{ML}$ as previously done in the folding studies of $NCBD_{Human}$
220 (*24*). This modification resulted in a thermodynamic stabilization of around 1 kcal mol^{-1}
221 for both $NCBD_{D/P}^{T2073W}$ and $NCBD_{Human}^{T2073W}$ (Fig. 6a-b, Supplementary Table S1).
222 Previous folding experiments were performed on a slightly longer $NCBD_{Human}$ variant
223 (residues 2058-2116), which was used in the original studies of CID/NCBD (*6*). In our
224 resurrection studies, we used a shorter version of $NCBD_{Human}$, only containing the
225 evolutionarily conserved region (residues 2062-2109). Therefore, we first repeated the
226 temperature-jump folding experiments for $NCBD_{Human}^{T2073W}$ and showed that the
227 shorter construct used in our evolutionary studies displayed similar kinetics as the
228 longer construct (Fig. 6c). We then performed folding experiments with
229 $NCBD_{D/P}^{T2073W}$. The kinetic transients of $NCBD_{D/P}^{T2073W}$ from temperature jump
230 experiments had lower signal-to-noise than those of $NCBD_{Human}^{T2073W}$, but observed
231 rate constants were in the same range (Fig. 6d). To investigate the folding kinetics
232 further we used stopped-flow fluorimetry, which has a lower time resolution but can be
233 used to compare folding rate constants for $NCBD_{D/P}^{T2073W}$ and $NCBD_{Human}^{T2073W}$ at low
234 temperature (Fig. 6e-f). The stopped-flow folding experiments were conducted by
235 making pH jumps from a 5 mM HCl solution (pH ~ 2) to a buffer solution of 20 mM
236 sodium phosphate (pH 7.4, 150 mM NaCl, 1 M TMAO) and monitoring the relaxation
237 through a 330 nm band-pass filter at 4°C. The low temperature is necessary to reduce

238 the observed rate constant such that the folding or other conformational transitions take
239 place in the millisecond time window. We observed two kinetic phases for
240 $NCBD_{Human}^{T2073W}$ (one fast phase with a negative amplitude and a second slower phase
241 with a positive amplitude) but only one kinetic phase for $NCBD_{D/P}^{T2073W}$ (with a
242 positive amplitude). The values of the observed rate constants for $NCBD_{Human}^{T2073W}$
243 (~300 s^{-1} and ~70 s^{-1}, respectively) were similar to those observed previously for the
244 longer construct (*24*). The single value obtained for the $NCBD_{D/P}^{T2073W}$ was ~140 s^{-1}.
245 Trp fluorescence is a very sensitive but crude structural probe. Thus, the number of
246 kinetic phases in folding experiments could be dependent on small structural
247 rearrangements around the Trp. Nevertheless, the observed rate constant for
248 $NCBD_{D/P}^{T2073W}$ in the stopped flow pH jump experiment is in the same range as the two
249 rate constants observed under the same conditions for human NCBD.
250
251
252 **Discussion**
253
254 The biophysics and molecular evolution of NCBD is interesting for several reasons,
255 which all relate to the dynamic properties of NCBD. Firstly, while it has a hydrophobic
256 core and globular shape, NCBD is a very dynamic protein domain with characteristics
257 of an IDP (*5*, *6*, *8–11*, *25*). Secondly, NCBD has several binding partners including the
258 three NCOA transcriptional co-regulator paralogs (*5*, *26*), the transcription factors p53
259 (*27*), Ets-2 (*28*) and interferon factor-3 (*29*), and viral proteins such as Tax (*30*) from
260 T-cell leukemia virus. Intriguingly, NCBD displays great conformational plasticity as
261 shown by its complex with interferon factor-3 where the helices of NCBD adopt a
262 distinct conformation as compared to the complex with CID (*31*). Thirdly, evolutionary

263 snapshots of the complex between CID and NCBD suggest that several new
264 intermolecular contacts and conformational plasticity increased the affinity when going
265 from the Cambrian-like $NCBD_{D/P}^{ML}$ (K_d ~ 1-5 μM) to younger variants (K_d ~ 0.2 μM)
266 (*12*, *13*, *32*). Fourthly, while affinity and structural order of modern NCBD/CID
267 complexes were increased, the transition state of the folding-induced binding displayed
268 more conformational heterogeneity as compared to the ancestral complex (*33*). Our
269 present results, how the free, unbound state of NCBD has evolved during the transition
270 from a low-affinity to a high-affinity CID binder relate to all four points.
271
272 The most striking finding is that $NCBD_{D/P}^{ML}$ displays very similar molten-globule like
273 properties as the previously characterized human NCBD (*8*, *10*). This conservation of
274 properties, borderline between a globular domain and an IDP, suggests that the
275 dynamics of NCBD is under positive selection and therefore of functional importance.
276 In general, structural plasticity is regarded as one main functional feature of IDPs
277 allowing for multiple protein-protein interactions (*34*). NCBD interacts with several
278 protein domains, both folded and disordered ones, and the dynamic nature of NCBD
279 likely increases its propensity to adapt to different partners. Moreover, NCBD
280 interactions result in coupled folding and binding. Many such reactions have recently
281 been shown to occur via a mechanism denoted templated folding, where the binding
282 partner influences the folding pathway (*35–37*). Indeed, this was observed for the
283 interaction between human NCBD and CID (*33*, *38*, *39*). Thus, our present findings
284 suggest that templated folding may be a general feature of binding reactions with
285 NCBD where the conserved dynamics facilitate sampling of free states, heterogeneity
286 of bound states, as well as the pathway between free and bound states.
287

288 Going into details of the NMR model, we note that while overall structure is robust to
289 errors in the predicted sequence as shown by the comparison of the NMR models of
290 free $NCBD_{D/P}^{ML}$ and $NCBD_{D/P}^{AltAll}$, there are differences in for example helix
291 orientations. Globular domains with a sequence identity as high as these NCBD variants
292 (77-88%) would typically have identical structures due to a highly funneled energy
293 landscape (*40*, *41*), while proteins with larger structural heterogeneity have less
294 funneled landscapes (*1*). Indeed, the differences between the structures of $NCBD_{Human}$,
295 $NCBD_{D/P}^{ML}$ and $NCBD_{D/P}^{AltAll}$, in particular regarding the angles of the helices in
296 relation to each other, are consistent with a less funneled energy landscape resulting in
297 conformational heterogeneity (*11*). This heterogeneity is also consistent with the
298 conserved dynamic properties of NCBD. In conclusion, our data suggest evolutionarily
299 conserved dynamics of NCBD that underlie functional plasticity in ground state
300 conformations, templated binding-and-folding and a propensity to interact with several
301 binding partners.
302
303
304 **Materials and methods**
305
306 **Protein sequences, expression and purification.** The reconstruction of ancestral
307 sequences was previously published (*12*). The AltAll versions of $NCBD_{D/P}$ (Fig. 1) and
308 CID_{1R} used in the present paper was based on posterior probabilities from the
309 reconstruction with a cutoff of 91%. One position in $NCBD_{D/P}$ (Thr2062) is very
310 uncertain. A Thr residue (15%) was originally chosen at this position in $NCBD_{D/P}^{ML}$ to
311 avoid a hydrophobic residue, although Ile (19%) has a higher posterior probability. In
312 the current $NCBD_{D/P}^{AltAll}$ residue 2062 is Ile. NCBD and CID variants were expressed

313 in *E. coli* from a pRSETA plasmid and purified as previously described (*33*)
314 Concentrations were determined by absorbance at 280 nm for NCBD (using calculated
315 extinction coefficients based on amino acid composition) or 205 nm for CID using an
316 extinction coefficient of 250,000 $M^{-1}cm^{-1}$. Purity was checked by SDS-PAGE and
317 identity of the purified proteins was confirmed by MALDI-TOF mass spectrometry.
318
319 **Circular dichroism**. Far-UV CD experiments were performed using a JASCO J-1500
320 CD spectrophotometer with a Peltier temperature control system. The protein
321 concentration in all CD experiments was 18-20 μM. The buffer solution was either 20
322 mM sodium phosphate (pH 7.4), 150 mM NaCl or 50 mM potassium formate (pH 3.0),
323 150 mM NaCl, and CD spectra were recorded at 277 K. The scanning speed was 50
324 nm/min, bandpass 1 nm and integration time 1 second. Each reported spectrum is an
325 average of 3-4 recorded spectra. In the equilibrium thermal denaturation experiments
326 the proteins were dissolved in 50 mM potassium formate buffer (pH 3.0), 150 mM NaCl
327 and the sample was heated from 277 to 368 K. The heating rate was 1 K/min, waiting
328 time 5 seconds and the denaturation was monitored at 222 nm. During the heating,
329 spectra (average of three measurements) were taken at 283, 303, 323, 343 and 363 K,
330 respectively. In the equilibrium urea denaturation experiments the proteins were
331 denatured in 0-6.6 M urea at 277 K and the unfolding was monitored at 222 nm. The
332 data was analyzed in GraphPad Prism and fitted by non-linear regression to a two-state
333 equilibrium model (*42*). Because of the broad unfolding transition and lack of native
334 baseline for several variants, four parameters were shared among all urea denaturation
335 data sets in the curve fitting (Fig. S4, Supplementary Table 1). One of these parameters
336 was the molar ellipticity of the native state, with the reasonable assumption that the
337 secondary structures of the native states are similar for all variants. The other

338 parameters were the slopes of the denatured and native baselines as well as the m_{D-N}
339 value (assuming a similar change in solvent accessible surface area upon denaturation
340 for all variants).
341
342 **Temperature jump experiments.** Temperature jump experiments were conducted
343 using 100-200 μM protein on a TJ-64 temperature jump system (TgK Scientific). The
344 buffer solution was 20 mM sodium phosphate (pH 7.4), 150 mM NaCl. The proteins
345 were subjected to temperature jumps of 2-8.5 K to different target temperatures. The
346 data were fitted in the Kinetic Studio software (TgK scientific) to a double exponential
347 function, to account both for the fast phase (relaxation time ~ 80 μs), which corresponds
348 to the heating time of the instrument, and to the slow phase, which corresponds to the
349 conformational transition in the protein. A Trp variant of $NCBD_{D/P}^{ML}$ ($NCBD_{D/P}^{T2073W}$)
350 was chosen for kinetic experiments since a Trp in this position was previously used for
351 human NCBD. We engineered a Trp at other positions in $NCBD_{D/P}^{ML}$ and obtained rate
352 constants in the same range for all variants (Supplementary Table S2).
353
354 **Stopped flow experiments.** The stopped flow experiments were performed using an
355 upgraded SX-17MV stopped flow spectrophotometer (Applied Photophysics) and the
356 measurements were conducted at 277 K. Proteins were dissolved in 5 mM HCl (pH ~
357 2) and rapidly mixed 1:1 with buffer solutions complemented with trimethylamine N-
358 oxide (TMAO) to a final concentration of 20 mM sodium phosphate (pH 7.4), 150 mM
359 NaCl, 1 M TMAO. The final protein concentration was 5 μM. The excitation
360 wavelength was 280 nm and the resulting fluorescence emission was detected after
361 passage through a 330 nm bandpass filter. The transients were analyzed in GraphPad
362 Prism and fitted to a single or double exponential function.

363

364 **NMR experiments**. NMR experiments were acquired on Bruker 600, 700 and 900
365 MHz spectrometers equipped with triple resonance cryogenic temperature probes at
366 298 K except otherwise stated. The final NMR samples contained 500 μM protein to
367 which 0.01% NaN_3 and 5% D_2O was added. Experiments for assignment and
368 subsequent structure determination were done at pH 2.4 (HCl adjusted with NaOH) for
369 $NCBD_{D/P}^{ML}$ and pH 6.8 for $NCBD_{D/P}^{AltAll}$. The following NMR experiments were
370 recorded for assignment and subsequent structure determination: standard 2D ^{1}H-^{15}N
371 HSQC, 3D HNCACB ^{15}N-resolved [^{1}H-^{1}H]-NOESY-HSQC, ^{15}N-TOCSY-HSQC ^{13}C-
372 resolved [^{1}H-^{1}H]-NOESY-HSQC, HCCH-TOCSY and ^{13}C-resolved [^{1}H-^{1}H]-TOCSY-
373 HSQC. Phi-angle restraining $^{3}J_{HNHA}$ couplings were determined from 3D HNHA type
374 experiments using quantitative -*J* intensity modulated experiments (*43*). The
375 temperature variation experiments were performed in 20 mM sodium formate, pH 3.0.
376 All experiments were processed with nmrpipe (*44*) and analysed with CCPnmr (*45*).

377

378 **Structure calculation**. Structure calculations were done using the CYANA 3.97 (*46*)
379 package as follows: Initially, cross peaks were converted into upper distance restraints
380 following an automated process in CYANA. These distance restraints together with
381 φ/ψ dihedral angles determined from C^{α}-chemical shifts and $^{3}J_{HNH}\alpha$ (measured) were
382 used as input for the initial structure calculations. The structures were calculated with
383 200,000 torsion angle dynamics steps for 100 conformers starting from random torsion
384 angles by simulated annealing. 20 conformers with the lowest target function values
385 were selected and analyzed. The structural statistics together with all input data for the
386 structure calculations are presented in Supplementary Table S3. Assignments and

387 structural coordinates have been deposited in the RCSB protein data bank with pdb
388 code: 7OSR (accession number BMRB ID 34635) ($NCBD_{D/P}^{ML}$) and 7OSW (accession
389 number BMRB ID 34636) ($NCBD_{D/P}^{AltAll}$).
390
391 **Acknowledgements**
392 This work was supported by the Wenner-Gren foundation WG-17 returning grants to
393 C. N. C., and by the Swedish Research Council (2020-04395 to P.J.) and Knut and
394 Alice Wallenberg foundation (Evolution of new genes and proteins, to P.J.). We used
395 the NMR Uppsala infrastructure, which is funded by the Department of Chemistry -
396 BMC and the Disciplinary Domain of Medicine and Pharmacy. We thank Magnus
397 Kjaergaard for valuable comments on the NMR experiments.
398
399

References

1. S. Gianni, M. I. Freiberger, P. Jemth, D. U. Ferreiro, P. G. Wolynes, M. Fuxreiter, Fuzziness and Frustration in the Energy Landscape of Protein Folding, Function, and Assembly. *Acc Chem Res*. **54**, 1251–1259 (2021).

2. O. F. Lange, N.-A. Lakomek, C. Farès, G. F. Schröder, K. F. A. Walter, S. Becker, J. Meiler, H. Grubmüller, C. Griesinger, B. L. de Groot, Recognition dynamics up to microseconds revealed from an RDC-derived ubiquitin ensemble in solution. *Science*. **320**, 1471–1475 (2008).

3. S. J. Wodak, E. Paci, N. V. Dokholyan, I. N. Berezovsky, A. Horovitz, J. Li, V. J. Hilser, I. Bahar, J. Karanicolas, G. Stock, P. Hamm, R. H. Stote, J. Eberhardt, Y. Chebaro, A. Dejaegere, M. Cecchini, J.-P. Changeux, P. G. Bolhuis, J. Vreede, P. Faccioli, S. Orioli, R. Ravasio, L. Yan, C. Brito, M. Wyart, P. Gkeka, I. Rivalta, G. Palermo, J. A. McCammon, J. Panecka-Hofman, R. C. Wade, A. Di Pizio, M. Y. Niv, R. Nussinov, C.-J. Tsai, H. Jang, D. Padhorny, D. Kozakov, T. McLeish, Allostery in Its Many Disguises: From Theory to Applications. *Structure*. **27**, 566–578 (2019).

4. H. J. Dyson, P. E. Wright, Role of Intrinsic Protein Disorder in the Function and Interactions of the Transcriptional Coactivators CREB-binding Protein (CBP) and p300. *J. Biol. Chem.* **291**, 6714–22 (2016).

5. C. H. Lin, B. J. Hare, G. Wagner, S. C. Harrison, T. Maniatis, E. Fraenkel, A small domain of CBP/p300 binds diverse proteins: solution structure and functional studies. *Mol Cell*. **8**, 581–590 (2001).

6. S. J. Demarest, M. Martinez-Yamout, J. Chung, H. Chen, W. Xu, H. J. Dyson, R. M. Evans, P. E. Wright, Mutual synergistic folding in recruitment of CBP/p300 by p160 nuclear receptor coactivators. *Nature*. **415**, 549–553 (2002).

7. M.-O. Ebert, S.-H. Bae, H. J. Dyson, P. E. Wright, NMR relaxation study of the complex formed between CBP and the activation domain of the nuclear hormone receptor coactivator ACTR. *Biochemistry*. **47**, 1299–308 (2008).

8. M. Kjaergaard, K. Teilum, F. M. Poulsen, Conformational selection in the molten globule state of the nuclear coactivator binding domain of CBP. *Proc. Natl. Acad. Sci. U.S.A.* **107**, 12535–12540 (2010).

9. M. Kjaergaard, F. M. Poulsen, K. Teilum, Is a malleable protein necessarily highly dynamic? The hydrophobic core of the nuclear coactivator binding domain is well ordered. *Biophys J*. **102**, 1627–1635 (2012).

10. M. Kjaergaard, L. Andersen, L. D. Nielsen, K. Teilum, A folded excited state of ligand-free nuclear coactivator binding domain (NCBD) underlies plasticity in ligand recognition. *Biochemistry*. **52**, 1686–1693 (2013).

11. E. Papaleo, C. Camilloni, K. Teilum, M. Vendruscolo, K. Lindorff-Larsen, Molecular dynamics ensemble refinement of the heterogeneous native state of NCBD using chemical shifts and NOEs. *PeerJ*. **6**, e5125 (2018).

12. G. Hultqvist, E. Åberg, C. Camilloni, G. N. Sundell, E. Andersson, J. Dogan, C. N. Chi, M. Vendruscolo, P. Jemth, Emergence and evolution of an interaction between intrinsically disordered proteins. *Elife*. **6**, e16059 (2017).

13. P. Jemth, E. Karlsson, B. Vögeli, B. Guzovsky, E. Andersson, G. Hultqvist, J. Dogan, P. Güntert, R. Riek, C. N. Chi, Structure and dynamics conspire in the evolution of affinity between intrinsically disordered proteins. *Sci. Adv.* **4**, eaau4130 (2018).

14. G. N. Eick, J. T. Bridgham, D. P. Anderson, M. J. Harms, J. W. Thornton, Robustness of Reconstructed Ancestral Protein Functions to Statistical Uncertainty. *Mol Biol Evol*. msw223 (2016).

15. K. M. Hart, M. J. Harms, B. H. Schmidt, C. Elya, J. W. Thornton, S. Marqusee, Thermodynamic system drift in protein evolution. *PLoS Biol*. **12**, e1001994 (2014).

16. L. Laursen, J. Čalyševa, T. J. Gibson, P. Jemth, Divergent Evolution of a Protein-Protein Interaction Revealed through Ancestral Sequence Reconstruction and Resurrection. *Mol Biol Evol*. **38**, 152–167 (2021).

17. P. D. Williams, D. D. Pollock, B. P. Blackburne, R. A. Goldstein, Assessing the accuracy of ancestral protein reconstruction methods. *PLoS Comput Biol*. **2**, e69 (2006).

18. V. A. Risso, J. A. Gavira, E. A. Gaucher, J. M. Sanchez-Ruiz, Phenotypic comparisons of consensus variants versus laboratory resurrections of Precambrian proteins. *Proteins*. **82**, 887–896 (2014).

19. M. L. Romero-Romero, V. A. Risso, S. Martinez-Rodriguez, B. Ibarra-Molero, J. M. Sanchez-Ruiz, Engineering ancestral protein hyperstability. *Biochem J*. **473**, 3611–3620 (2016).

20. D. L. Trudeau, M. Kaltenbach, D. S. Tawfik, On the Potential Origins of the High Stability of Reconstructed Ancestral Proteins. *Mol Biol Evol*. **33**, 2633–2641 (2016).

21. L. C. Wheeler, S. A. Lim, S. Marqusee, M. J. Harms, The thermostability and specificity of ancient proteins. *Curr Opin Struct Biol*. **38**, 37–43 (2016).

22. T. W. Hearing, T. H. P. Harvey, M. Williams, M. J. Leng, A. L. Lamb, P. R. Wilby, S. E. Gabbott, A. Pohl, Y. Donnadieu, An early Cambrian greenhouse climate. *Sci Adv*. **4**, eaar5690 (2018).

23. T. Wotte, C. B. Skovsted, M. J. Whitehouse, A. Kouchinsky, Isotopic evidence for temperate oceans during the Cambrian Explosion. *Sci Rep*. **9**, 6330 (2019).

476 24. J. Dogan, A. Toto, E. Andersson, S. Gianni, P. Jemth, Activation Barrier-Limited
477 Folding and Conformational Sampling of a Dynamic Protein Domain.
478 *Biochemistry*. **55**, 5289–5295 (2016).

479 25. S. J. Demarest, S. Deechongkit, H. J. Dyson, R. M. Evans, P. E. Wright, Packing,
480 specificity, and mutability at the binding interface between the p160 coactivator
481 and CREB-binding protein. *Protein Sci.* **13**, 203–210 (2004).

482 26. J. Xu, Q. Li, Review of the in vivo functions of the p160 steroid receptor
483 coactivator family. *Mol. Endocrinol.* **17**, 1681–1692 (2003).

484 27. J. A. Livengood, K. E. S. Scoggin, K. Van Orden, S. J. McBryant, R. S.
485 Edayathumangalam, P. J. Laybourn, J. K. Nyborg, p53 Transcriptional activity is
486 mediated through the SRC1-interacting domain of CBP/p300. *J Biol Chem*. **277**,
487 9054–9061 (2002).

488 28. G. Jayaraman, R. Srinivas, C. Duggan, E. Ferreira, S. Swaminathan, K.
489 Somasundaram, J. Williams, C. Hauser, M. Kurkinen, R. Dhar, S. Weitzman, G.
490 Buttice, B. Thimmapaya, p300/cAMP-responsive element-binding protein
491 interactions with ets-1 and ets-2 in the transcriptional activation of the human
492 stromelysin promoter. *J Biol Chem*. **274**, 17342–17352 (1999).

493 29. S. Matsuda, J. C. Harries, M. Viskaduraki, P. J. F. Troke, K. B. Kindle, C. Ryan,
494 D. M. Heery, A Conserved alpha-helical motif mediates the binding of diverse
495 nuclear proteins to the SRC1 interaction domain of CBP. *J Biol Chem*. **279**,
496 14055–14064 (2004).

497 30. K. E. Scoggin, A. Ulloa, J. K. Nyborg, The oncoprotein Tax binds the SRC-1-
498 interacting domain of CBP/p300 to mediate transcriptional activation. *Mol Cell*
499 *Biol*. **21**, 5520–5530 (2001).

500 31. B. Y. Qin, C. Liu, H. Srinath, S. S. Lam, J. J. Correia, R. Derynck, K. Lin, Crystal
501 structure of IRF-3 in complex with CBP. *Structure*. **13**, 1269–1277 (2005).

502 32. E. Karlsson, A. Lindberg, E. Andersson, P. Jemth, High affinity between
503 CREBBP/p300 and NCOA evolved in vertebrates. *Protein Sci.* **29**, 1687–1691
504 (2020).

505 33. E. Karlsson, C. Paissoni, A. M. Erkelens, Z. A. Tehranizadeh, F. A. Sorgenfrei, E.
506 Andersson, W. Ye, C. Camilloni, P. Jemth, Mapping the transition state for a
507 binding reaction between ancient intrinsically disordered proteins. *J Biol Chem*.
508 **295**, 17698–17712 (2020).

509 34. P. E. Wright, H. J. Dyson, Intrinsically disordered proteins in cellular signalling
510 and regulation. *Nat Rev Mol Cell Biol*. **16**, 18–29 (2015).

511 35. A. Toto, C. Camilloni, R. Giri, M. Brunori, M. Vendruscolo, S. Gianni, T. A, C.
512 C, G. R, B. M, V. M, G. S., Molecular Recognition by Templated Folding of an
513 Intrinsically Disordered Protein. *Sci. Rep.* **6**, 21994 (2016).

36. A. Toto, F. Malagrinò, L. Visconti, F. Troilo, L. Pagano, M. Brunori, P. Jemth, S. Gianni, Templated folding of intrinsically disordered proteins. *J. Biol. Chem.* **295**, 6586–6593 (2020).

37. D. Wu, H.-X. Zhou, W. D, Z. HX., Designed Mutations Alter the Binding Pathways of an Intrinsically Disordered Protein. *Sci. Rep.* **9**, 6172 (2019).

38. P. Jemth, X. Mu, Å. Engström, J. Dogan, A frustrated binding interface for intrinsically disordered proteins. *J. Biol. Chem.* **289**, 5528–5533 (2014).

39. E. Karlsson, E. Andersson, J. Dogan, S. Gianni, P. Jemth, C. Camilloni, A structurally heterogeneous transition state underlies coupled binding and folding of disordered proteins. *J. Biol. Chem.* **294**, 1230–1239 (2019).

40. C. Chothia, A. M. Lesk, The relation between the divergence of sequence and structure in proteins. *EMBO J.* **5**, 823–826 (1986).

41. M. Oliveberg, P. G. Wolynes, The experimental survey of protein-folding energy landscapes. *Q. Rev. Biophys.* **38**, 245–288 (2005).

42. A. Fersht, *Structure and mechanism in protein science: a guide to enzyme catalysis and protein folding.* (Macmillan, 1999).

43. N.-A. Lakomek, J. Ying, A. Bax, Measurement of ^{15}N relaxation rates in perdeuterated proteins by TROSY-based methods. *J Biomol NMR*. **53**, 209–221 (2012).

44. F. Delaglio, S. Grzesiek, G. W. Vuister, G. Zhu, J. Pfeifer, A. Bax, NMRPipe: a multidimensional spectral processing system based on UNIX pipes. *J Biomol NMR*. **6**, 277–293 (1995).

45. W. F. Vranken, W. Boucher, T. J. Stevens, R. H. Fogh, A. Pajon, M. Llinas, E. L. Ulrich, J. L. Markley, J. Ionides, E. D. Laue, The CCPN data model for NMR spectroscopy: development of a software pipeline. *Proteins*. **59**, 687–696 (2005).

46. P. Güntert, C. Mumenthaler, K. Wüthrich, Torsion angle dynamics for NMR structure calculation with the new program Dyana. *J. Mol. Biol.* **273**, 283–298 (1997).

544 **Figures**

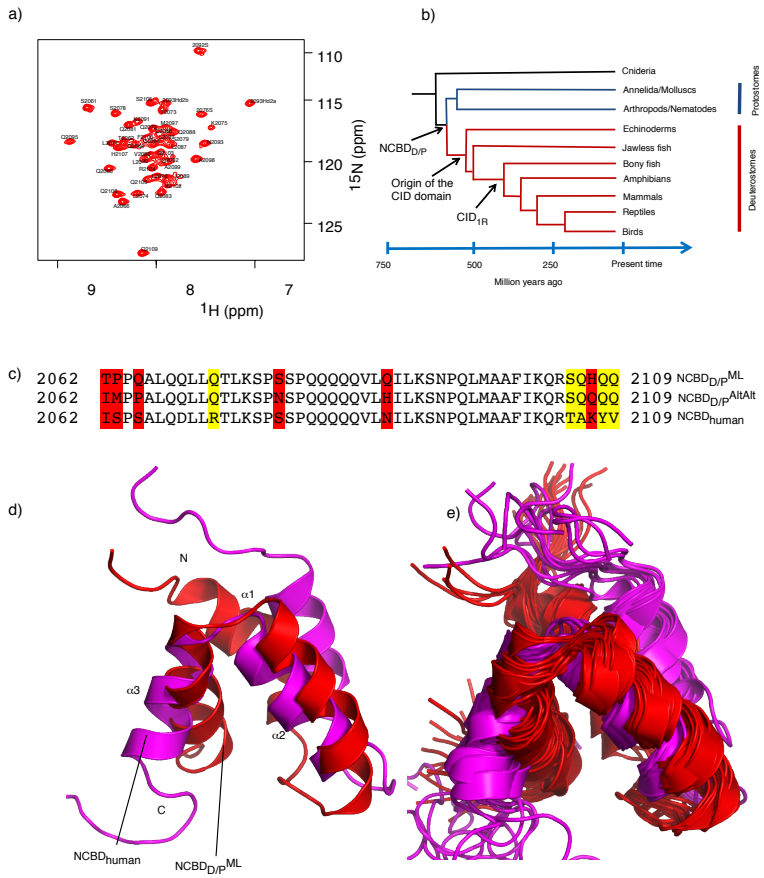

545

546 **Figure 1. Structures of ancestral and human NCBD domains**. (a) ^{1}H-^{15}N HSQC
547 spectrum of $NCBD_{D/P}^{ML}$ at pH 2.4 with assigned residues. All assignments and the
548 structural coordinates have been deposited in the pdb data bank with accession
549 number BMRB ID 34635 and pdb code: 7OSR. (b) A schematic tree depicting the
550 relationship between the deuterostome/protostome (D/P) ancestor and modern
551 species. The times on the x-axis are approximate, in particular the divergence of
552 protostomes and deuterostomes. (c) Sequence alignment for $NCBD_{Human}$, $NCBD_{D/P}^{ML}$
553 $NCBD_{D/P}^{AltAlt}$. The residues differing between $NCBD_{D/P}^{ML}$ and $NCBD_{D/P}^{AltAlt}$ are
554 marked in red while additional differences to $NCBD_{Human}$ are marked in yellow. (d)
555 Comparison of the NMR structure of ancestral $NCBD_{D/P}^{ML}$ solved at low pH (red, pdb
556 code: 7OSR), and the previously determined human NCBD (magenta, 2KKJ) (*8*).

Note that the structure of human NCBD was solved using a slightly longer construct.

(e) Overlay of the 20 lowest energy structures of the $NCBD_{D/P}^{ML}$ domain with those of $NCBD_{human}$.

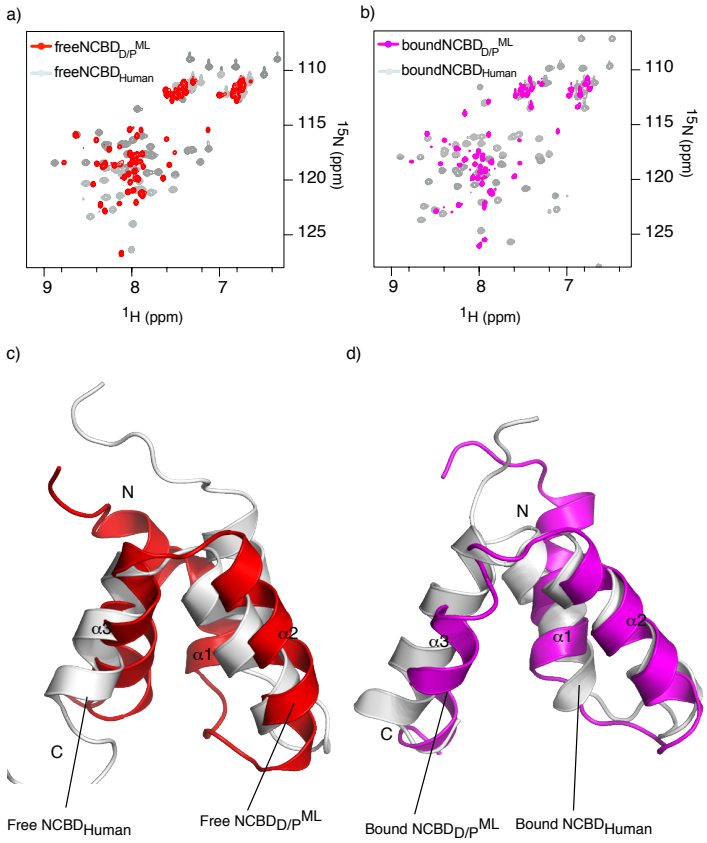

Figure 2. Comparison of the ligand-free and bound ancestral NCBD$_{D/P}^{ML}$ and extant NCBD$_{Human}$. The ligand-bound conformations (pdb codes 6ES5 and 6ES7) and the structure of free human NCBD (pdb code: 2KKJ) (*8*) were previously determined. (a) Overlay of the ^{1}H-^{15}N HSQC spectra between free NCBD$_{D/P}^{ML}$ (red) and free NCBD$_{Human}$ (grey). (b) Overlay of the ^{1}H-^{15}N HSQC spectra between CID-bound NCBD$_{D/P}^{ML}$ (magenta) and CID-bound NCBD$_{Human}$ (grey). Structural alignment between (c) free NCBD$_{D/P}^{ML}$ (red, 7OSR) and free NCBD$_{Human}$ (grey, 2KKJ), and (d) CID-bound NCBD$_{D/P}^{ML}$ (magenta, , 6ES5) and CID-bound NCBD$_{Human}$ (grey, 6ES7).

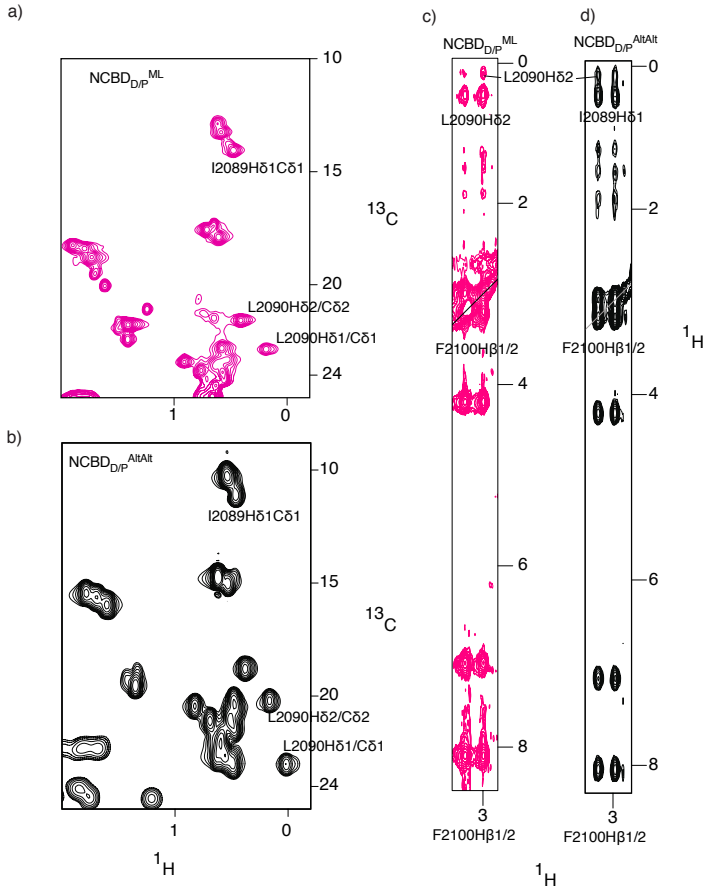

Figure 3. Phe2100 makes NOEs to Ile2089 and Leu2090 in NCBD$_{D/P}^{ML}$ and NCBD$_{D/P}^{AltAlt}$. (a) ^{1}H-^{13}C HSQC spectra of the methyl region of NCBD$_{D/P}^{ML}$, showing the Hδ1-Cδ1 shifts of L2090 and I2089. (b) ^{1}H-^{13}C HSQC spectra of the methyl region of NCBD$_{D/P}^{AltAlt}$, showing the Hδ1-Cδ1 shifts of L2090 and I2089. (c) Strip from a ^{1}H-^{1}H ^{13}C resolved NOESY showing NOEs from the Hβ1/2 atoms of Phe2100 and the associated NOEs to Leu2090Hδ1 for NCBD$_{D/P}^{ML}$. (d) Strip from a ^{1}H-^{1}H ^{13}C resolved NOESY showing NOEs from the Hβ1/2 atoms of Phe2100 and the associated NOEs to Leu2090Hδ1 and Ile2089Hδ1 for NCBD$_{D/P}^{AltAlt}$. These signature NOEs implies that both proteins form a hydrophobic core similar to that of NCBD$_{Human}$.

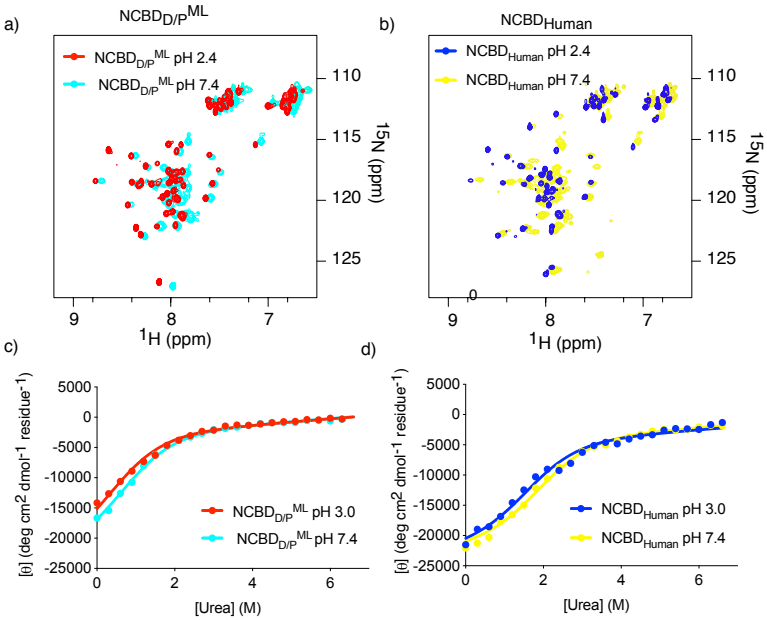

Figure 4. Comparison of ancestral NCBD$_{D/P}^{ML}$ and extant NCBD$_{Human}$ at two different pH values. a) Overlay of the ^{1}H-^{15}N HSQC spectra of NCBD$_{D/P}^{ML}$ at pH 2.4 (red) and at pH 6.8 (cyan). b) Overlay of the ^{1}H-^{15}N HSQC spectra of NCBD$_{Human}$ at pH 2.4 (blue) and at pH 6.8 (yellow). c) Urea denaturation experiments for NCBD$_{D/P}^{ML}$ at pH 3.0 (red) and at pH 7.4 (cyan). d) Urea denaturation experiments for NCBD$_{Human}$ at pH 3.0 (yellow) and at pH 7.4 (blue).

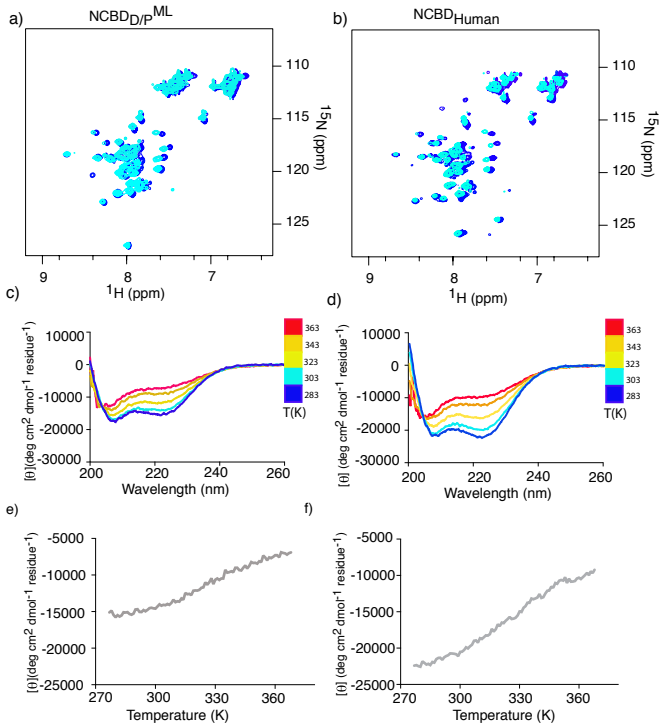

Figure 5. Temperature dependence for ancestral NCBD$_{D/P}^{ML}$ and extant human NCBD. a) Overlay of ^{1}H-^{15}N HSQC spectra of NCBD$_{D/P}^{ML}$ at 283 K (blue) and at 303 K (cyan). b) Overlay of ^{1}H-^{15}N HSQC spectra of NCBD$_{Human}$ at 283 K (blue) and at 303 K (cyan). Circular dichroism spectra at a range of temperatures (283-363 K) for (c) NCBD$_{D/P}^{ML}$ and (d) NCBD$_{Human}$. Molecular ellipticity at 222 nm (probing α-helix content) as a function of temperature for (e) NCBD$_{D/P}^{ML}$ and (f) NCBD$_{Human}$.

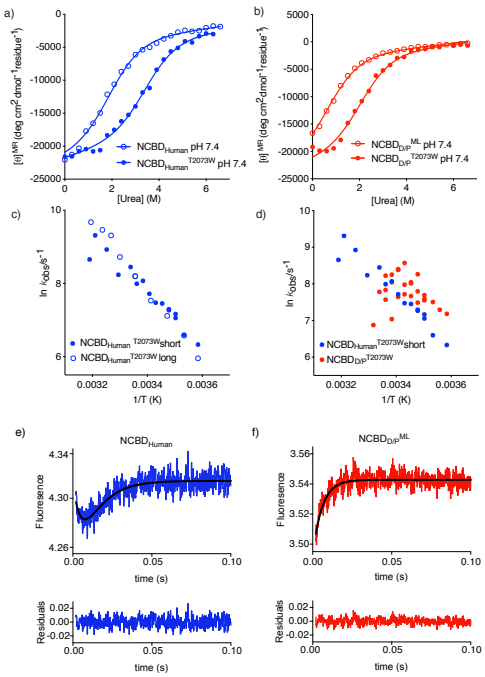

598

599 **Figure 6. Stability and temperature dependence of kinetic rate constants for**

600 **NCBD$_{D/P}^{ML}$ and extant human NCBD.** (a) Stability measurement of NCBD$_{Human}^{WT}$

601 (open circles) and NCBD$_{Human}^{T2073W}$ (filled circles) measured by urea denaturation.

602 (b) Stability measurement of NCBD$_{D/P}^{ML}$ (open circles) and NCBD$_{D/P}^{T2073W}$ (filled

603 circles). Parameters from the curve fitting are shown in Supplementary Table S1. (c)

604 Temperature jump kinetic experiments for a longer human NCBD construct used in

605 previous studies (*24*) (open circles) and the shorter human NCBD variant used in this

606 study (filled circles). Both variants contained the T2073W mutation. (d) A

607 comparison of observed rate constants from temperature-jump experiments for

608 NCBD$_{Human}^{T2073W}$ (blue) and NCBD$_{D/P}^{T2073W}$ (red). All experiments were performed

609 in 20 mM sodium phosphate pH 7.4, 150 mM NaCl. (e-f) Kinetic (un)folding of

610 NCBD$_{Human}^{T2073W}$ and NCBD$_{D/P}^{T2073W}$ measured by stopped flow fluorescence

611 spectroscopy. (e) (Un)folding kinetic transient of NCBD$_{Human}^{T2073W}$ (blue) fitted to a

612 double exponential function (black line). Below each transient are the residuals from

613 the respective fits. (f) Stopped flow (un)folding kinetic transient of NCBD$_{D/P}^{T2073W}$

614 (red) fitted to a single exponential function (black line). The experiments were

615 performed by jumping from 5 mM HCl (pH ~ 2) to a final buffer concentration of 20

616 mM sodium phosphate (pH 7.4), 150 mM NaCl, 1 M TMAO. The relaxation was

617 monitored using a 330 band-pass emission filter. Fitting a double exponential function

618 resulted in k_{obs} values of 290 ± 30 and 67 ± 4 s^{-1} for $NCBD_{Human}^{T2073W}$. Fitting a single

619 exponential function yielded a k_{obs} value of 139 ± 7 s^{-1} for $NCBD_{D/P}^{T2073W}$.

620

621

Supplementary information

The dynamic properties of a nuclear coactivator binding domain are evolutionarily conserved

Elin Karlsson[1], Frieda A. Sorgenfrei[1,†], Eva Andersson[1], Jakob Dogan[1], Per Jemth[1,*], and Celestine N. Chi[1,2,*]

[1]Department of Medical Biochemistry and Microbiology, Uppsala University, BMC Box 582, SE-75123 Uppsala, Sweden.

[2]Department of Pharmaceutical Biosciences, Uppsala University, BMC Box 582, SE-75123 Uppsala, Sweden

[†]Present address: acib GmbH, Krenngasse 37, 8010 Graz c/o University of Graz, Institute of Chemistry, NAWI Graz, BioTechMed Graz, Heinrichstrasse 28, 8010 Graz, Austria

*Correspondence to

Celestine Chi, Celestine.Chi@imbim.uu.se

Per Jemth, Per.Jemth@imbim.uu.se

Supplementary figures

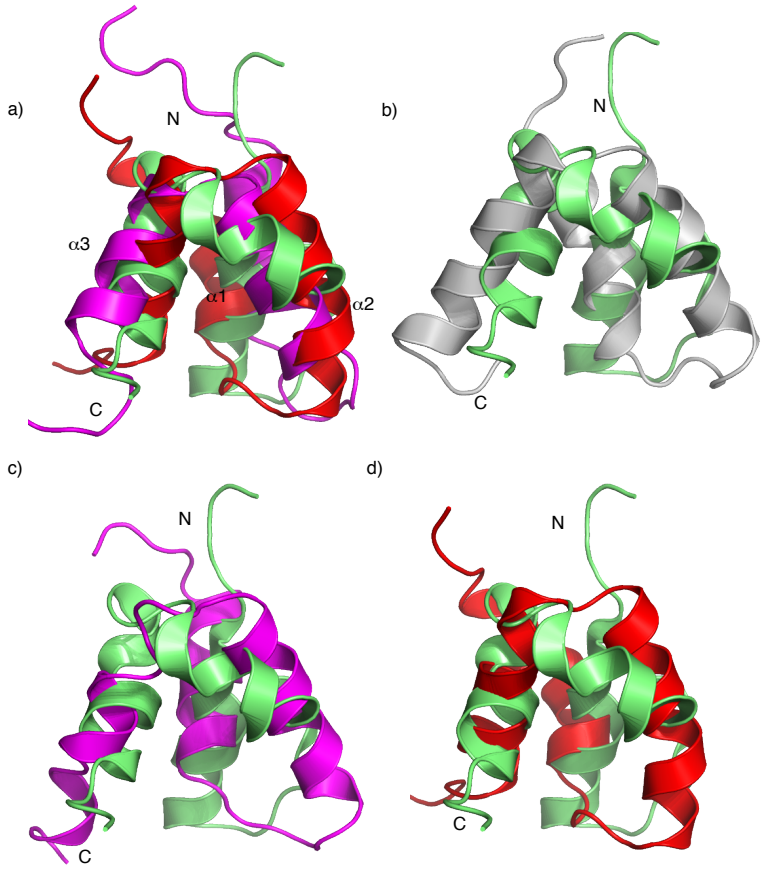

Figure S1. Overlay of the structures of $NCBD_{D/P}^{ML}$, $NCBD_{D/P}^{AltAlt}$ and $NCBD_{Human}$. (a) An overlay of the structures determined from NMR for $NCBD_{D/P}^{ML}$(red, pdb code: 7OSR), $NCBD_{D/P}^{AltAlt}$ (green, 7OSW), and the previously determined $NCBD_{Human}$ (magenta, 2KKJ). (b) Overlay of $NCBD_{D/P}^{AltAlt}$ (green, 7OSW), and the previously determined CID-bound $NCBD_{D/P}^{ML}$ (grey, 6ES5). (c) Overlay of $NCBD_{D/P}^{AltAlt}$ (green, 7OSW), and the previously determined $NCBD_{Human}$ (magenta, 2KKJ). (d) Overlay of $NCBD_{D/P}^{AltAlt}$ (green, 7OSW) and $NCBD_{D/P}^{ML}$ (red, 7OSR).

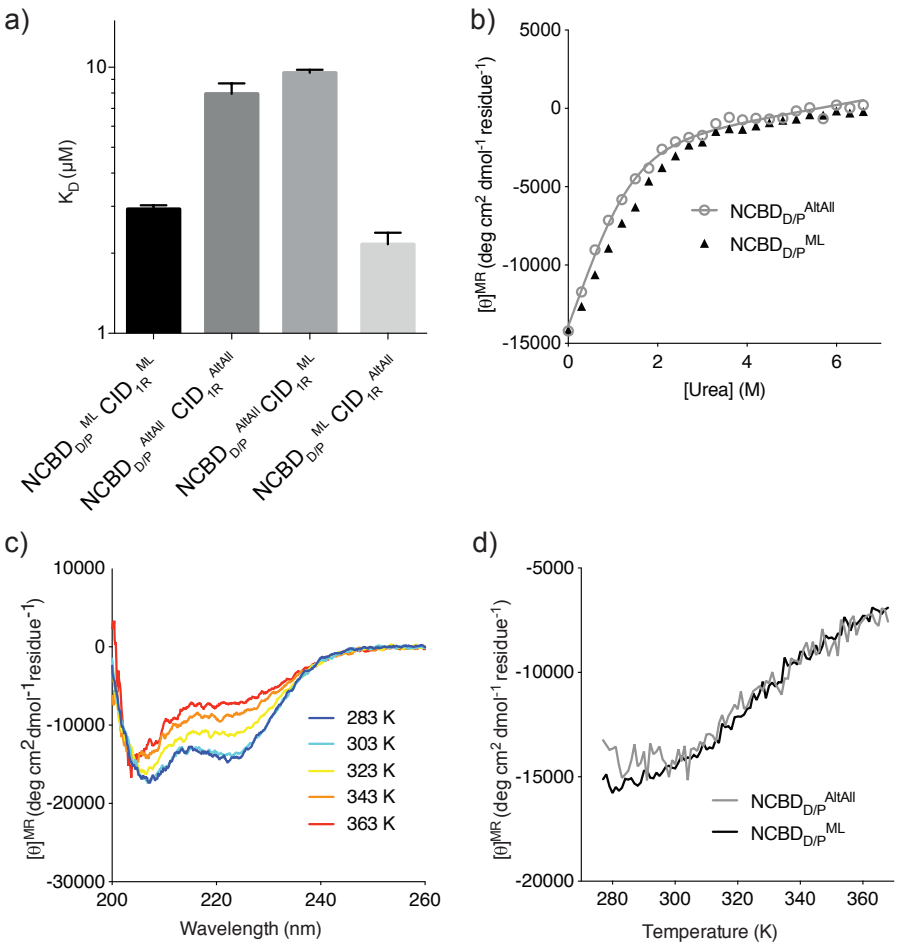

Figure S2. The biophysical properties of NCBD$_{D/P}^{ML}$ are robust to errors in the sequence. a) Binding affinities of NCBD$_{D/P}^{ML}$ or NCBD$_{D/P}^{AltAlt}$ and CID$_{1R}^{ML}$ or CID$_{1R}^{AltAll}$ measured with ITC. The buffer solution was 20 mM sodium phosphate pH 7.4, 150 mM NaCl. (b) Stability of NCBD$_{D/P}^{AltAll}$ measured by urea denaturation in 50 mM formate (pH 3.0), 150 mM NaCl. The CD signal at 222 nm was monitored and the data was fitted to a two-state function. A reliable [urea]$_{50\%}$ value could not be obtained, although qualitative comparison with NCBD$_{D/P}^{ML}$ indicates that the stability of the two variants is similar. (c-d) Temperature stability for NCBD$_{D/P}^{AltAll}$. The CD signal at 222 nm was monitored and spectra were taken at temperatures 283-363 K.

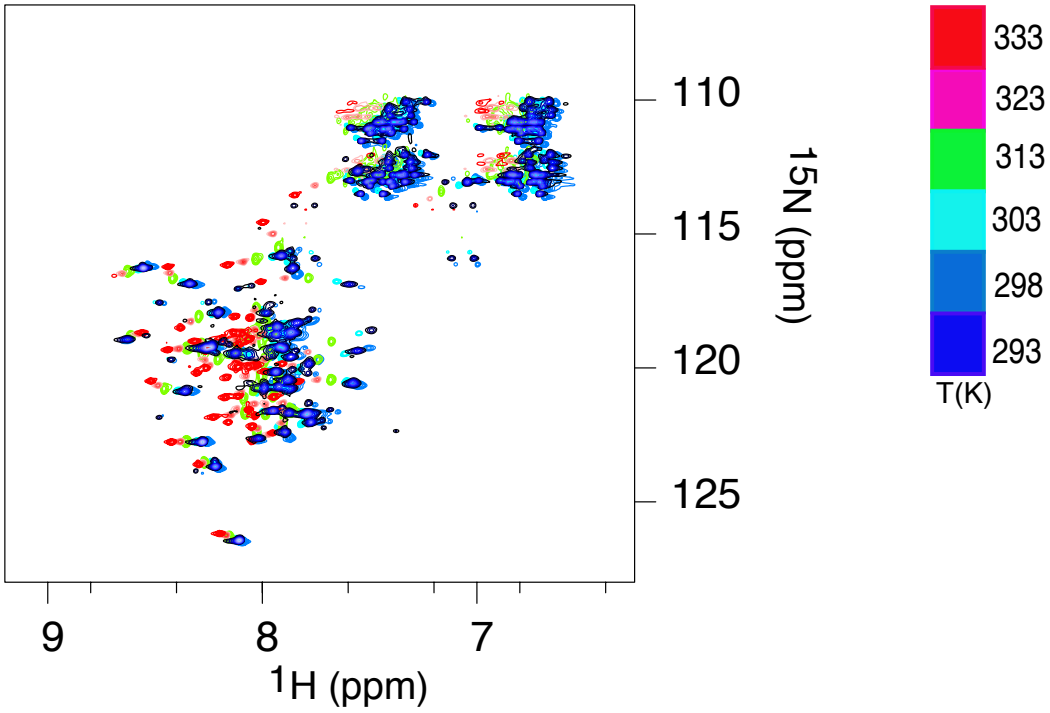

Figure S3. ^{15}N-^{1}H HSQC spectra of NCBD$_{D/P}^{ML}$ at different temperatures. The experiments were performed from 293 K (blue) to 333 K (red).

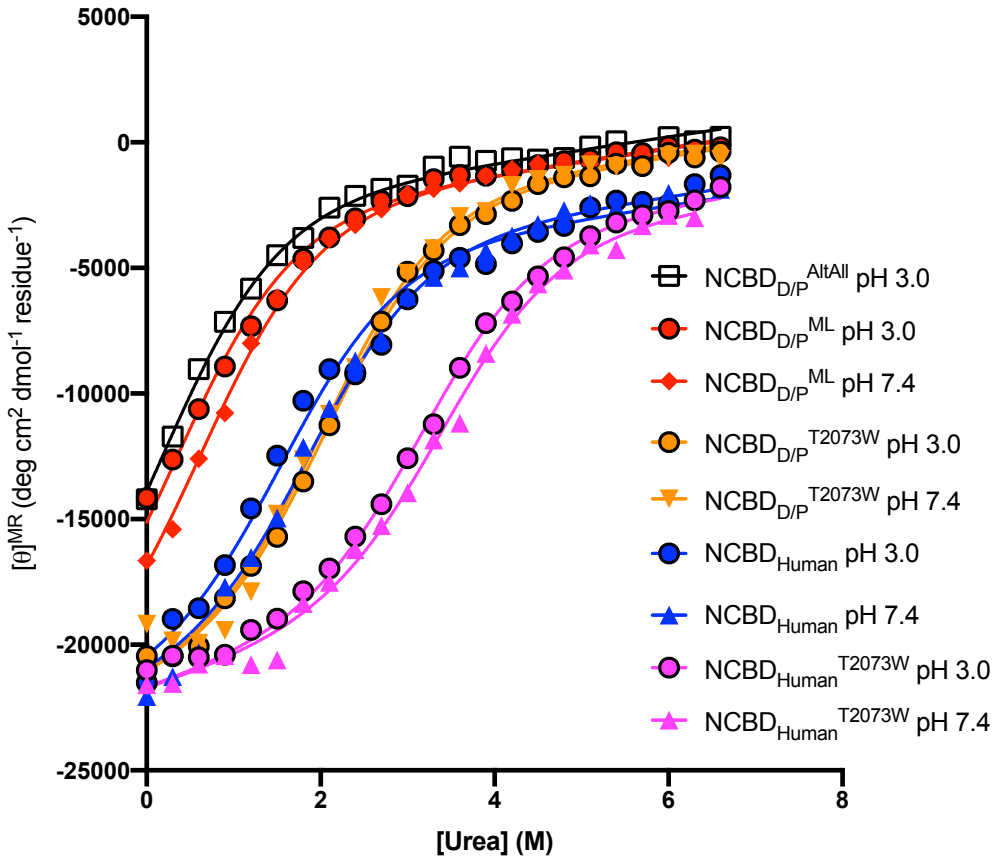

Figure S4. Equilibrium urea denaturation experiments. All data sets were fitted simultaneously to a two-state model in GraphPad Prism with shared parameters for the native state molar ellipticity, the denatured and native baseline slopes and the $m_{D\text{-}N}$ value. Experiments were performed in either 50 mM potassium formate buffer (pH 3.0), 150 mM NaCl or 20 mM sodium phosphate buffer (pH 7.4), 150 mM NaCl. The shared $m_{D\text{-}N}$ value was fitted as 0.74 ± 0.07 kcal $mol^{-1}M^{-1}$.

Supplementary Tables

Supplementary Table S1. Stabilities of NCBD variants expressed as the urea concentration at 50% denaturation. The proteins were denatured with urea and the structural transition was monitored with CD at 222 nm at 277 K. The solutions were either 50 mM potassium formate buffer (pH 3.0), 150 mM NaCl or 20 mM sodium phosphate buffer (pH 7.4), 150 mM NaCl. The data were fitted to a two-state model in GraphPad Prism. The parameters for the signal of the native state, the denatured and native baseline slopes, and the $m_{D\text{-}N}$ value were shared among the data sets in the curve fitting to allow fitting of the low stability $NCBD_{D/P}^{ML}$ and $NCBD_{D/P}^{AltAll}$ variants. The shared $m_{D\text{-}N}$ value was fitted as 0.82 ± 0.025 kcal $mol^{-1}M^{-1}$. The errors are the standard error from the curve fitting and likely a low estimate of.

Variant	**pH**	**$[Urea]_{50\%}$ (M)**	**$\Delta G_{D\text{-}N}$ (kcal/mol)**
$NCBD_{D/P}^{AltAll}$	3.0	0.22 ± 0.04	0.18 ± 0.03
$NCBD_{D/P}^{ML}$	3.0	0.38 ± 0.04	0.31 ± 0.03
$NCBD_{D/P}^{ML}$	7.4	0.68 ± 0.04	0.55 ± 0.04
$NCBD_{D/P}^{T2073W}$	3.0	2.13 ± 0.04	1.73 ± 0.06
$NCBD_{D/P}^{T2073W}$	7.4	2.08 ± 0.04	1.70 ± 0.06
$NCBD_{Human}$	3.0	1.61 ± 0.04	1.31 ± 0.05
$NCBD_{Human}$	7.4	1.94 ± 0.05	1.58 ± 0.06
$NCBD_{Human}^{T2073W}$	3.0	3.24 ± 0.07	2.64 ± 0.10
$NCBD_{Human}^{T2073W}$	7.4	3.46 ± 0.08	2.82 ± 0.11

Supplementary Table 2. Rate constants and kinetic amplitudes of folding for different D/P NCBD Trp variants measured in temperature jump experiments. The experiments were conducted using 200 μM protein in 20 mM sodium phosphate (pH 7.4), 150 mM NaCl. The jump in temperature was from 277 to 285.5 K.

Variant	**Amplitude**	k_{obs} **(s^{-1})**
$NCBD_{D/P}^{T2073W}$	1.06 ± 0.06	2400 ± 200
$NCBD_{D/P}^{L2067W}$	0.91 ± 0.02	1530 ± 50
$NCBD_{D/P}^{S2078W}$	0.35 ± 0.01	700 ± 60
$NCBD_{D/P}^{H2107W}$	0.47 ± 0.02	820 ± 80
$NCBD_{D/P}^{Q2108W}$	0.73 ± 0.02	960 ± 60

Supplementary Table 3

	$NCBD_{D/P}^{ML}$	$NCBD_{D/P}^{AltAlt}$
NMR distance and dihedral restraints		
Distance restraints		
Total NOEs	329	347
Intra-residue	113	145
Sequential ($\|i-j\| = 1$)	122	111
Medium-range ($1 < \|i-j\| < 4$)	76	76
Long-range ($\|i-j\| > 5$)	18	39
Total dihedral angle restraints	76	63
$^{3}J_{HN\alpha}$ scalar couplings	39	43
$^{13}C^{\alpha}$ chemical shifts	100	100
Structure statistics		
Average CYANA target function value ($Å^2$)	2.5 ± 0.2	2.8 ± 0.3
Violations		
Distance constraints (>0.5 Å)	0	0
Dihedral angle constraints (>5°)	0	0
Deviations from idealized geometry		
Bond lengths (Å)	0	0
Bond angles (°)	0	0
Impropers (°)	0	0
Average pairwise r.m.s. deviation (Å)		
Backbone residues	2.2 ± 1.0	0.5 ± 0.2
Heavy atoms residues	2.7 ± 1.0	1.0 ± 0.3